Driving Triplet State Population in Benzothioxanthene Imide Dyes: Let's twist!

Darío Puchán Sánchez, Pierre Josse, Nathan Plassais, Geonwoo Park, Yeasin Khan, Yejoo Park, Mathilde Seinfeld, Antoine Guyard, Magali Allain, Frédéric Gohier, et al.

Chemistry–A European Journal
Research Article
doi.org/10.1002/chem.202400191
Chemistry Europe
European Chemical Societies Publishing
www.chemeurj.org

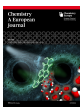

Driving Triplet State Population in Benzothioxanthene Imide Dyes: Let's twist!

Darío Puchán Sánchez,[a] Pierre Josse,[a] Nathan Plassais,[a, b] Geonwoo Park,[c] Yeasin Khan,[d] Yejoo Park,[d] Mathilde Seinfeld,[e] Antoine Guyard,[c] Magali Allain,[a] Frédéric Gohier,[a] Lhoussain Khrouz,[e] Dominik Lungerich,[f, g] Hyun S. Ahn,[c] Bright Walker,[d] Cyrille Monnereau,*[e] Clément Cabanetos,*[a, h] and Tangui Le Bahers*[e, i]

Controlling the formation of photoexcited triplet states is critical for many (photo)chemical and physical applications. Here, we demonstrate that a permanent out-of-plane distortion of the benzothioxanthene imide (BTI) dye promotes intersystem crossing by increasing spin-orbit coupling. This manipulation was achieved through a subtle chemical modification, specifically the bay-area methylation. Consequently, this simple yet efficient approach expands the catalog of known molecular engineering strategies for synthesizing heavy atom-free, dual redox-active, yet still emissive and synthetically accessible photosensitizers.

Introduction

Considering the critical role of triplet excited states in various applications such as photodynamic therapy (PDT),[1] photocatalysis,[2] molecular logic gates,[3] catalytic hydrogen production[4] or triplet-triplet-annihilation (TTA) up-conversion,[5] to promote and control intersystem crossing (ISC) in visible to infra-red light absorbing molecules have attracted considerable attention. While the most reported approaches consist of functionalizing π-conjugated systems with heavy atoms (ruthenium, iridium, iodine, and bromine) to enhance the spin-orbit coupling (SOC),[6] their inherent drawbacks (dark toxicity, lifetimes of the photogenerated triplet-state, prices, *etc.*) have pushed the community to consider other options, particularly for biological and medicinal applications.[7] Consequently, various design principles have emerged to promote triplet state generation. For example, n–π*↔π–π* transitions (to fulfill the El-Sayed rule),[8] S_1-T_n state energy matching (reduction of the gap),[9] exciton coupling,[10] or ISC by charge recombination (CS-ISC),[11] spin-orbit charge-transfer (SOCT-ISC)[12] or through the deformation (twisting) of the π-conjugated backbone have all been demonstrated so far.[13] Though efficient,[14] syntheses of these molecular systems are usually achieved through time-consuming and sometimes synthetically demanding processes. Hence, as a step toward structural accessibility, the simple thionation of imide-based chromophores/ π-conjugated scaffolds was recently demonstrated as an accessible strategy to afford remarkably effective triplet-harvesting photosensitizers (PSs).[15] Despite being efficient in providing a high ISC, this post-functionalization faces limitations: thionated compounds lack photostability, as the back conversion of the thione into the carbonyl is observed under continuous light irradiation and in the presence of oxygen. Moreover, the complete quenching of their emission, resulting from the thionation, prohibits their in-situ tracking (bioimaging). Consequently, providing a synthetically accessible/cost-effective platform that is easily func-

[a] D. Puchán Sánchez, P. Josse, N. Plassais, M. Allain, F. Gohier, C. Cabanetos
Univ Angers, CNRS, MOLTECH-ANJOU, SFR MATRIX, F-49000 Angers, France
E-mail: clement.cabanetos@univ-angers.fr
[b] N. Plassais
Department of Physics, University of Seoul, 02504, Seoul, Republic of Korea
[c] G. Park, A. Guyard, H. S. Ahn
Yonsei University, 50 Yonsei-ro, Seodaemun-gu, 03722 Seoul, Republic of Korea
[d] Y. Khan, Y. Park, B. Walker
Department of Chemistry, Kyung Hee University, 730-701 Seoul, Republic of Korea
[e] M. Seinfeld, L. Khrouz, C. Monnereau, T. Le Bahers
ENS de Lyon, CNRS, Laboratoire de Chimie UMR 5182, F-69342 Lyon, France
E-mail:;
E-mail: cyrille.monnereau@ens-lyon.fr
tangui.le_bahers@ens-lyon.fr
[f] D. Lungerich
Center for Nanomedicine, Institute for Basic Science (IBS), IBS Hall, 50 Yonsei-ro, Seodaemun-gu, Seoul, 03722, South Korea
[g] D. Lungerich
Department of Nano Biomedical Engineering (NanoBME), Advanced Science Institute, Yonsei University, 50 Yonsei-ro, Seodaemun-gu, Seoul, 03722, South Korea
[h] C. Cabanetos
2BFUEL, IRL CNRS 2002, Yonsei University, 50 Yonsei-ro, Seodaemun-gu, 03722 Seoul, Republic of Korea
[i] T. Le Bahers
Institut Universitaire de France, 5 rue Descartes, 75005 Paris, France

Supporting information for this article is available on the WWW under https://doi.org/10.1002/chem.202400191

tionalizable (to fine-tune its optoelectronic properties), combining intersystem crossing and significant residual luminescence while displaying excellent photochemical stability, is still a major challenge.

In recent years, we have focused on the benzothioxanthene imide (**BTI**) structure,[16] a sulfur-containing rylene, and particularly on the regio- and chemo-selective functionalization of its π-conjugated backbone. Rationalization of the structure-property relationships revealed remarkable and tuneable optoelectronic properties through subtle and generally synthetically accessible chemical modifications.[17] While the native **BTI** molecule constitutes an outstanding fluorophore, with a quantum yield reaching almost unity, manipulation of the ISC kinetics was demonstrated by controlling the nature and positions of the substituents[15b,18] and/or simultaneously varying the nature and oxidation state of the constituting heteroatoms.[19] Stemming from a large spin-vibronic coupling itself activated by the distortion of the π-system, the sulfonation of the **BTI** was indeed found to be, for instance, an effective strategy to drive triplet formation.[15b] However, this post-functionalization also resulted in a significant blue shift of the absorption, turning the **BTI** into a weak absorber in the visible spectral region. Hence, to circumvent this limitation, we report herein the synthesis and characterization of a new derivative, entitled **MBTI**, in which a methyl group was inserted in the bay region of the dye (Figure 1).

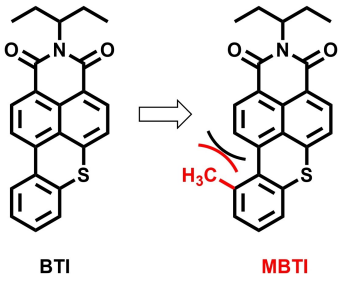

Figure 1. Structures and concept to promote ISC, i.e., the selective methylation of the bay to induce a permanent distortion of the π-system.

This minimalist yet selective functionalization is indeed expected to induce enough permanent distortion to the π-conjugated backbone to promote singlet to triplet conversion through increased spin-orbit coupling.[20] Sometimes called twisting-induced triplet state population in the literature,[21] this elegant strategy is currently attracting significant attention, particularly for preparing the next generation of heavy-atom-free photosensitizers.[22]

Results and Discussion

With the explicit goal of synthetic accessibility, the methyl-functionalized **MBTI** was successfully prepared in only two steps from affordable and commercially available starting materials using a strategy adapted from our recently reported optimized synthesis of the **BTI** (Scheme 1).[23]

The preparation of **MBTI** was thus initiated with the treatment of 2-amino-4-methylbenzothiazole under basic conditions to generate the reactive 2-amino-3-methylbenzenethiol that was directly utilized in a one-pot reaction with the 4-bromo-1,8-naphthalic anhydride.[13b] Through the successive addition of isoamyl nitrite and 3-aminopentane, the target imide-based derivative was isolated, characterized by mass spectrometry (see SI), and subsequently characterized by nuclear magnetic resonance (NMR) spectroscopy in deuterated chloroform (Figure 2-A).

Beyond the expected disappearance of a signal in the aromatic region (hydrogen annotated "e" on the **BTI** structure), the impact of the methyl group on the structure of the dye (steric hindrance) can be directly monitored by the consequent shielding of the signal related to the naphthyl hydrogen annotated "c". The structural deformation of **MBTI**, anticipated by DFT calculations, was thereafter confirmed by single crystal X-ray diffraction and compared to its almost flat parent compound (Figure 2-B and 2-C). While **BTI** shows a torsion

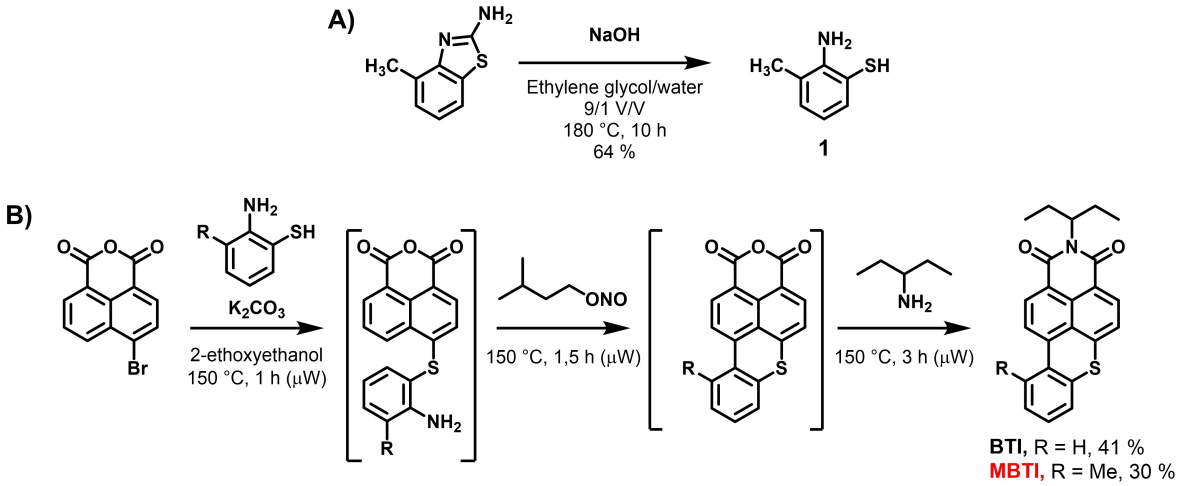

Scheme 1. Synthesis of the 2-amino-3-methylbenzenethiol precursor (A) and the two benzothioxanthene imide derivatives compared in this study (B), namely **BTI** and **MBTI**.

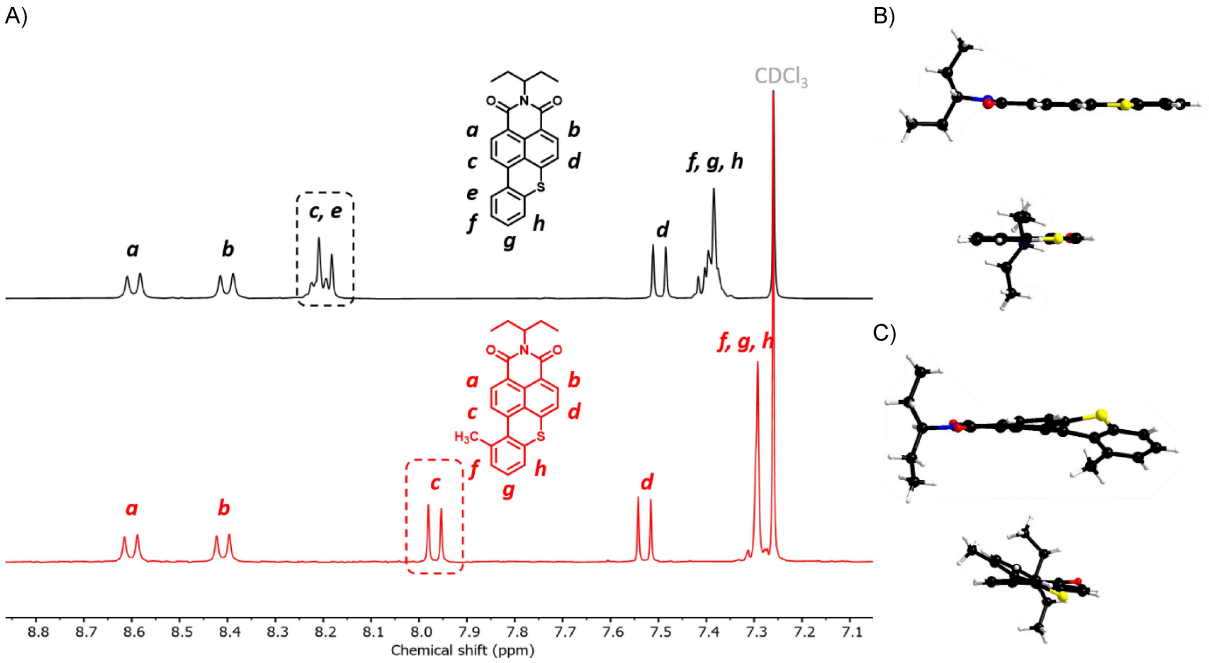

Figure 2. A) Comparison of the NMR spectra of **BTI** (black, top) and **MBTI** (red, bottom), recorded in $CDCl_3$ at room temperature. The **BTI** (B) and **MBTI** (C) structures were solved by X-ray diffraction on single crystals grown by slow evaporation technique.

angle between the upper naphthylamide and the lower phenyl moiety of *ca* 2°, the presence of the methyl group in the bay region of **MBTI** results in a significant increase of the latter to *ca* 24°. To assess the impact of this functionalization on the optoelectronic properties, both compounds were characterized by cyclic voltammetry (Figure 3-A).

The cyclic voltammogram of **MBTI** was recorded in CH_2Cl_2 using Bu_4NPF_6 as a supporting electrolyte. A reversible redox profile similar to that of the **BTI** was observed for **MBTI**, with the difference being a slight shift of the anodic and cathodic peak potentials (E_{pa} and E_{pc}, respectively). Careful comparison reveals that the positive inductive effect caused by the methyl group in **MBTI** and, to some extent, the deformation of its backbone results in a slight reduction of the electrochemical gap (of *ca* 20 mV, Table 1).

With minor changes recorded on the cyclic voltammetry, the effect of this chemical functionalization also appeared, at first glance, limited on the optical properties. Visually indistinguishable solutions of each dye in CH_2Cl_2 were subsequently analyzed by UV-visible absorption spectroscopy (Figure 3-B and Table 1). While almost similar onsets were recorded, **MBTI** was found to be devoid of the vibronic shoulder at 478 nm, characteristic of its planar analog (**BTI**), suggesting reorganization processes of (slightly) higher amplitude between the ground and excited state and a somewhat more pronounced intramolecular charge transfer (ICT) character of the transition. TD-DFT calculations further confirmed this feature by computing a higher charge transfer distance (D_{CT}) for the **MBTI** (1.9 Å vs 1.6 Å for **BTI**).[24] Despite a slight hypsochromic effect, the impact of the methylation on the absorption profiles appears, overall, negligible. In stark contrast, significant differences were monitored by spectroelectrochemistry (Figures 3, C, and D). While radical species of the **BTI** exhibit distinct spectral signatures with a λ_{max} at 903 nm for its radical cation and a bathochromically shifted structured absorption band characterized by an onset at *ca* 1190 nm for its radical anion, those of the methylated derivative appear almost superimposable in the low energy region with λ_{max} centered around 980 nm. These features suggest reorganization processes between the ground and excited state of different amplitude for the **BTI** (affecting the conjugation along the backbone, and thus the ground-to-excited state energetic gap) while within the same order for the

Table 1. Electrochemical and optical properties.

Molecule	E_{pa} (V)	E_{pc} (V)	λ_{max} absorption (nm)	ε ($M^{-1}cm^{-1}$)	λ_{max} emission (nm)	Φ_f (%)[a]	τ_{obs} (ns)	k_r (s^{-1})	k_{nr} (s^{-1})	Φ_Δ (%)[b]
BTI	1.26	−1.75	457	22360	509	99	7.48	1.3×10^8	1.3×10^6	<1
MBTI	1.22	−1.73	463	18500	514	70	7.25	9.7×10^7	4.1×10^7	8

[a] Φ_f = fluorescence quantum yield, measured using Coumarin-153 as reference (Φ_f = 0.45 in MeOH). [b] Φ_Δ = singlet oxygen quantum yield, measured using Phenalenone as reference (Φ_Δ = 0.95 in CH_2Cl_2).

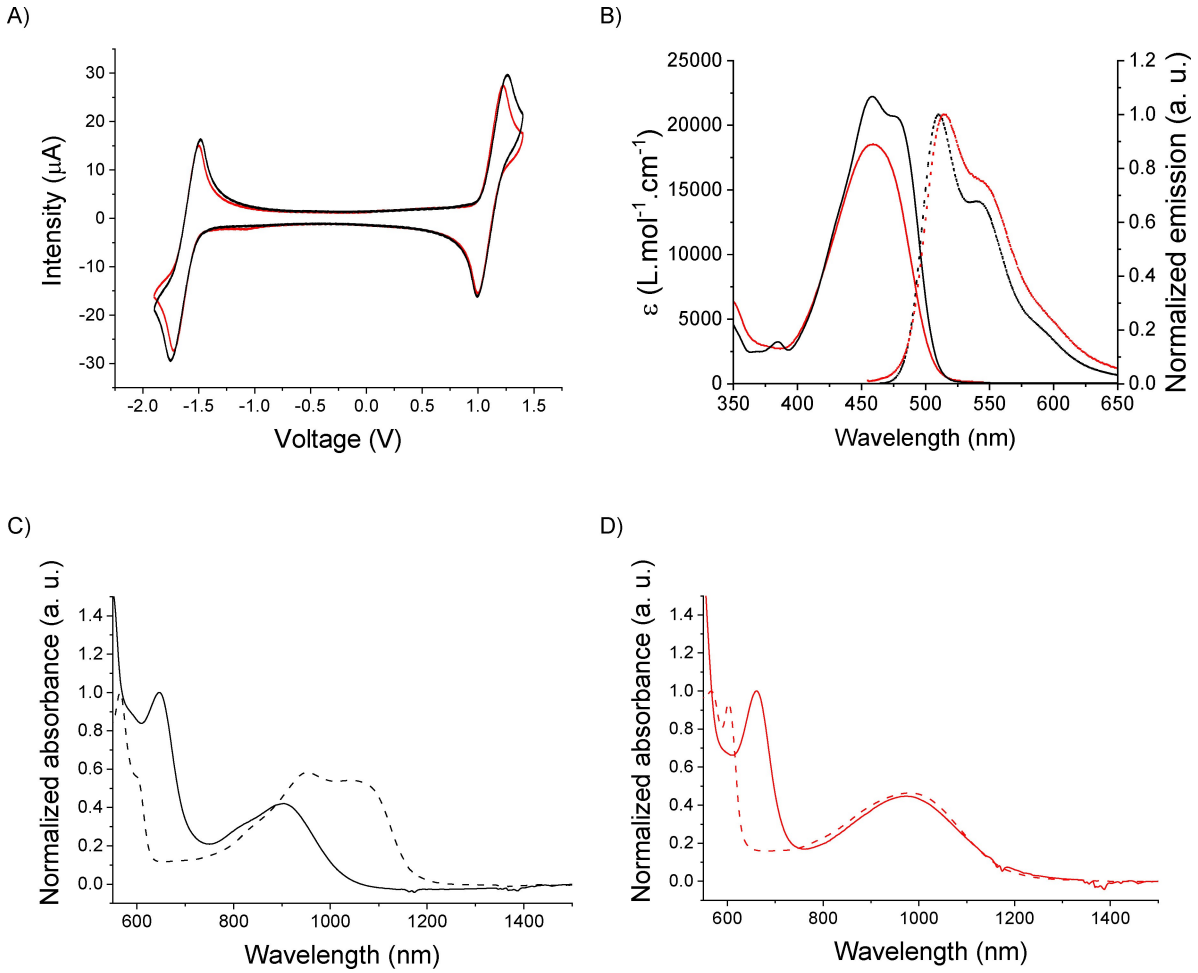

Figure 3. A) Cyclic voltammogram of **BTI** (black) and **MBTI** (red) recorded in CH_2Cl_2 at 100 mV s^{-1} using Bu_4NPF_6 as supporting electrolyte. B) Normalized absorption (solid line) and emission (dotted line) spectra of **BTI** (black) and **MBTI** (red) in CH_2Cl_2. Optical spectra of the radical cation (solid) and radical anion (dash) of **BTI** (C) and **MBTI** (D) recorded in CH_2Cl_2 using 0.1 M LiTFSI as supporting electrolyte.

already twisted **MBTI**. This is further confirmed by DFT calculations performed on the native, oxidized and reduced forms of **BTI** and **MBTI**. The radical cation is computed more planar than the native form with an associated torsion angle of 0° for **BTI** and 21.4° for **MBTI** (vs 7° for BTI and 26° for MBTI in the native state). The radical anion is more twisted than the native form with associated torsion angles of 13.9° for BTI and 27.8° for MBTI. The TD-DFT simulated absorption spectra (provided in Supporting Information) of the oxidized forms are in good agreement with experimental ones. The absorption in the NIR is associated to a charge transfer transition (D_{CT} = 2.1 Å) and the electronic transition close to 600 nm is due to a more localized transition (D_{CT} = 1.1 Å) for both compounds. The agreement is less satisfactory for the reduced form (radical anion) with a computed first transition not as red-shifted as the experimental one in the case of **BTI**. Regarding the emission properties, similar profiles, and Stokes shifts were monitored for both derivatives, with a slight shift of the emission maxima of 5 nm. However, quantifying the fluorescence highlighted a significant difference between the two compounds with a drop of quantum yield (QY) from almost unity to *ca* 70% upon methylation. This increase of non-radiative de-excitation kinetics is probably due to the added methyl that brings new molecular motions able to dissipate energy such as C–H vibration, methyl rotation or twisting of the π-system. As a matter of fact, the activation energy for the π-system distortion can be estimated from a relaxed scan at the S_1 state along the dihedral angle and brings a value close to 10 kJ mol^{-1} (see Supporting Information). In addition to this increase in non-radiative de-excitation kinetics, intersystem crossing (ISC) was also demonstrated by measuring a non-negligible singlet oxygen generation quantum yield (φ_Δ of *ca* 8% for **MBTI** *vs.* less than 1% for **BTI**). Supported by quantum chemical modeling, this feature was correlated to a significant increase of the spin-orbit coupling stemming from the methyl group that induces a distortion of the π-system (Figure 4). To support more this hypothesis, the SOC has been computed for different torsion angle (obtained by a TD-DFT relaxed scan at the S_1 potential energy surface) both for MBTI and BTI (Figure S9). It clearly shows that a flat conformation (an angle of 0°) does not experience an intense SOC while a twisting induces an increase of the SOC. Since the BTI molecule is more stable for a flat conformation and the MBTI more stable

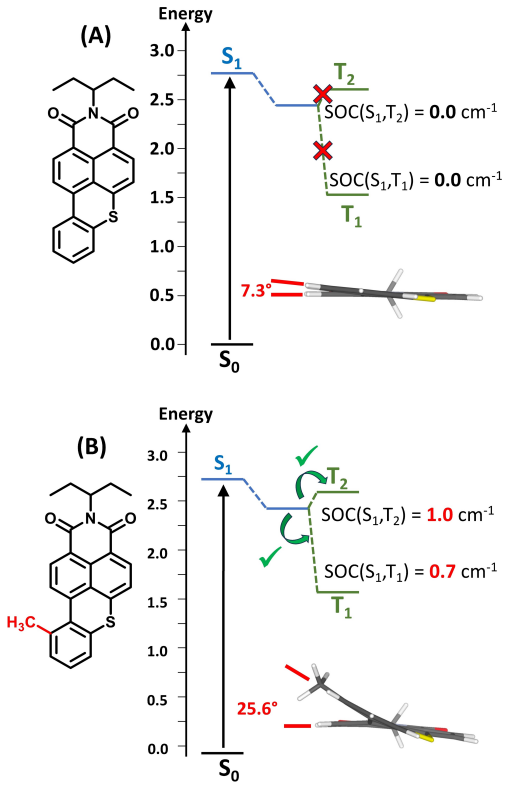

Figure 4. Comparison of the computed electronic states of **BTI** (A) and the methyl-functionalized **MBTI** (B). The spin-orbit couplings between S_1 and T_n states were computed at the S_1 geometry. Ground state computed distortion of the geometry is presented in inset.

for a twisted conformation, the MBTI experiences a larger SOC between S_1 and T_1.

Electron paramagnetic resonance (EPR) measurements were carried out in parallel, revealing a clear signature of the nitroxide radical of the 2,2,6,6-tetramethyl-4-piperidine (TEMP).[25] In agreement with the photophysical characterizations, the reaction with singlet oxygen was thus highlighted for both compounds but with distinct kinetics ($k_{MBTI} > 2k_{BTI}$, Figure 5-A and Figure S11).

Subsequently, another spin-trap, the 5,5-dimethyl-1-pyrroline-*N*-oxide (DMPO), was used to investigate the potential photogeneration of other reactive oxygen species (ROS).[26] Simulation of the experimental data, plotted in Figure 5, revealed that while a clear and unique signature assigned to the generation of superoxide ($O_2^{-\bullet}$) radical was monitored for **MBTI** (g = 2.0064, aN = 12.9G, aH = 10.1G, aH = 1.4G, Figure 5-C), two species were, at least, detected for **BTI** (Fig 5-B) corresponding to the superoxide anion, as the major one ($O_2^{-\bullet}$,g = 2.0064, aN = 13.1G, aH = 10.1G, aH = 1.1G, 85 %), associated to a unidentified O-centered radical alkoxy ($RO^{\bullet}$, g = 2.0062, aN = 13.8G, aH = 8G, aH = 1.6G,15 %).[27] These different evidence of multiple pathways towards radical oxygen species photoactivation led to the investigation of possible hydrogen peroxide (photo)generation by square wave voltammetry (SWV) and double differential pulse amperometry (DDPA) experiments, carried out at the interface of an irradiated biphasic aqueous (phosphate-buffered saline) and dye-based organic solution (**BTI** or **MBTI** in CH_2Cl_2, Figure 6).

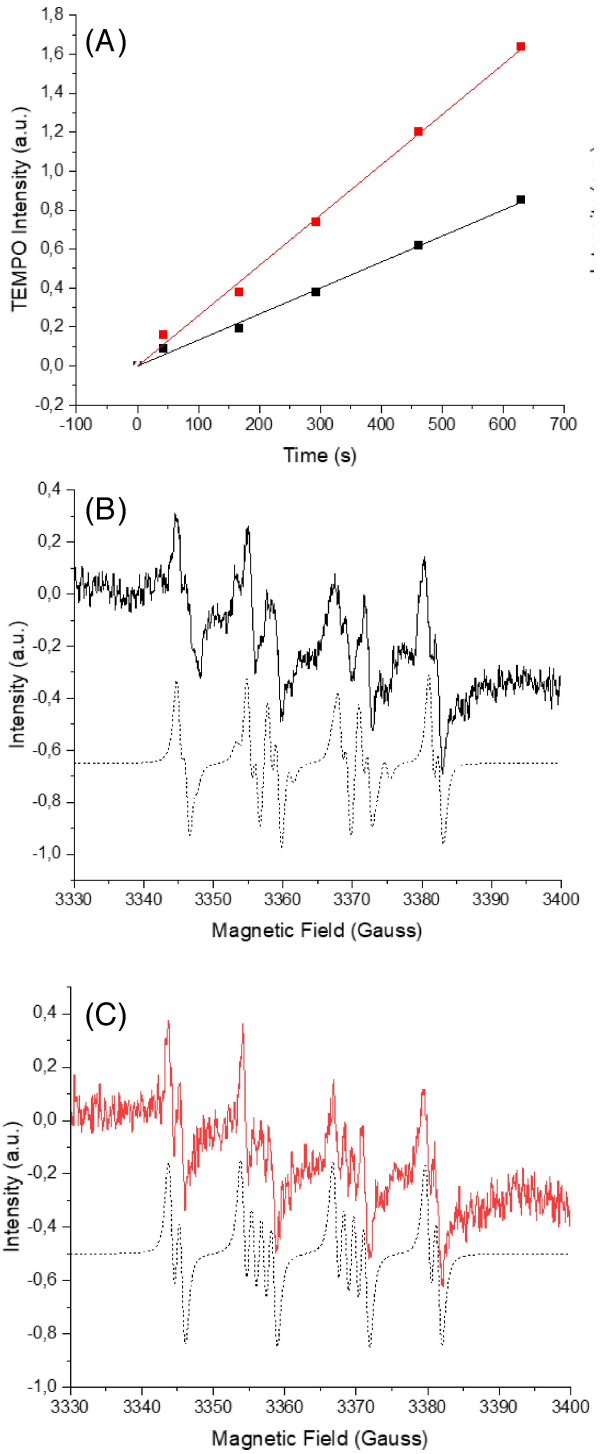

Figure 5. A) integration of the EPR signals related to the conversion of **TEMP** into **TEMPO** (g = 2.006, aN = 15.9 G) through reaction with the photo-generated singlet oxygen upon gradual irradiation for BTI (black squares) and **MBTI** (red squares) in similar operating conditions. Linear fits (black and red line, respectively) indicate an approximately twice as fast conversion for **MBTI**. Experimental EPR signals recorded in DMSO solution of **BTI** (B, black line) and **MBTI** (C, red line) after 15 min of irradiation at 455 nm in the presence of **DMPO**, along with the simulated ones (grey, dashed).

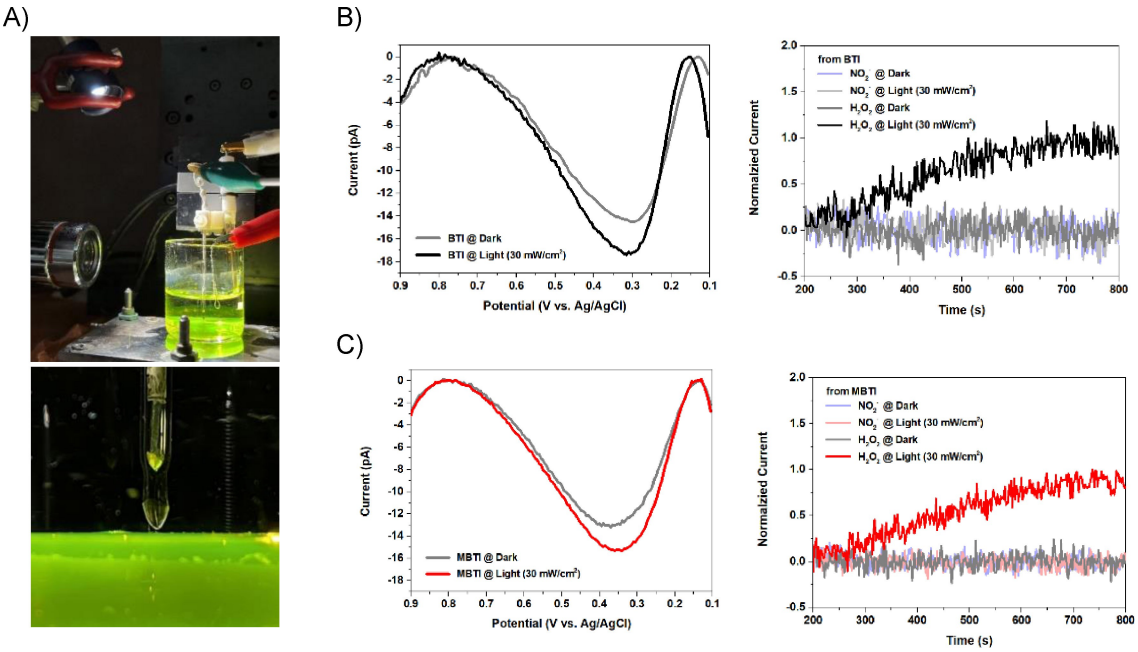

Figure 6. A) Illustration of the setup used to detect the photogeneration of H_2O_2 at the interface: a platinum ultramicroelectrode (Pt UME) with a diameter of 10 μm was used as a working electrode, Ag/AgCl (1 M KCl) and a Pt wire as the reference and counter electrode respectively. Square-wave voltammograms and evolution of the H_2O_2 production of BTI (B) and MBTI (C) solubilized in CH_2Cl_2 in the dark or under an irradiation @30 mW/cm^2 by square wave voltammetry (SWV) and double differential pulse amperometry (DDPA).

In addition to demonstrating a noticeable photoproduction of H_2O_2 for both compounds, it turns out that **BTI** was found to be slightly more efficient than its methylated counterpart ($\Phi H_2O_2 = 25.8$ ppm *vs* $\Phi H_2O_2 = 15.2$ ppm for **MBTI**). Albeit not fully rationalized, several contributions from the literature report that the common preceding process to either H_2O_2 or singlet oxygen both rely on the population of triplet state from ISC.[28] With potentially two competitive processes, and in consistency with EPR measurements, the lower H_2O_2 photoproduction of **MBTI** can thus be correlated to its improved propensity to sensitize molecular oxygen dissolved in the solution.

Conclusions

Through a slight chemical modification, consisting of the simple methylation of the bay area of the **BTI** dye, we contribute herein to refining our understanding of the closely intertwined connection between spin-orbit coupling, distortion of the π-system, and intersystem crossing. While only minor effects are observed in the cyclic voltammetry, and UV-visible absorptivity, non-negligible singlet oxygen sensitization was evidenced in this heavy-atom-free, dual redox-active, emissive, and synthetically accessible dye class. The formation of hydrogen peroxide reported for the two compounds proves that the mechanism of triplet state population is not completely understood and an estimation of the ISC efficiency and kinetics by transient spectroscopy for instance could provide valuable information. However, this work points out that a careful selection of the nature and size of the substituent used to functionalize the bay area of the **BTI** appears to be an appealing strategy to fine-tune the optoelectronic properties as well as spin-orbit coupling in this system, paving the road to promising perspective in terms of design principle and scope of applications.

Experimental section

General methods: All reagents and chemicals from commercial sources were used without further purification unless specified. Solvents were dried and purified using standard techniques. Flash chromatography was performed with analytical-grade solvents using ALDRICH silica gel (technical grade, pore size 60 Å, 230–400 mesh particle size). Flexible plates ALUGRAM Xtra SIL G UV254 from MACHEREY-NAGEL were used for TLC. Compounds were detected by UV irradiation (BIOBLOCK SCIENTIFIC). Nuclear Magnetic Resonance (NMR) spectra were recorded with a BRUKER AVANCE III 300 (^{1}H, 300 MHz and ^{13}C, 75 MHz) or a BRUKER AVANCE DRX500 (^{1}H, 500 MHz and ^{13}C, 125 MHz). Chemical shifts are given in ppm relative to the residual ^{1}H resonance of the deuterated solvent and coupling constants *J* in Hz. High Resolution Mass Spectrometry (HRMS) was performed with a JEOL JMS-700 B/E. Matrix Assisted Laser Desorption/Ionization was performed on MALDI-TOF MS BIFLEX III Bruker Daltonics spectrometer using DCTB+ as matrix (Bruker, Billerica, MA, USA). Absorption spectra were recorded on a JASCO V-650 spectrophotometer in diluted solution (ca. 10–5 or 10–6 mol L^{-1}), using spectrophotometric grade solvents. Emission spectra were measured using Horiba-Jobin-Yvon Fluorolog-3 fluorimeter. The steady-state luminescence was excited by unpolarized light from a 450 W xenon continuous wave (CW) lamp and detected at an angle of 90° for measurements of dilute solutions (10 mm quartz cuvette) by using a Hamamatsu R928. Cyclic voltammetry was performed using a Biologic SP-150 potentiostat with positive feedback compensation in 0.1 M Bu_4NPF_6/CH_2Cl_2 (HPLC grade) under an inert atmosphere (Ar) using a glovebox. Experiments were

carried out at a concentration of 10^{-3} M in a one-compartment cell equipped with a glassy carbon working electrode (2 mm of diameter), a platinum wire counter electrode and a $Ag/AgNO_3$ reference electrode. In all the experiments, the scan rate was 100 mV s^{-1}. EPR spectra were performed with 10^{-4} M solutions of each photosensitizers and either 2,2,6,6-tetramethyl-4-piperidine (TEMP) (Sigma-Aldrich) at 5 10^{-3} M in $CHCl_3$ solution or DMPO[1] (TCI chemicals) at 5 10^{-3} M in DMSO solution. Samples were prepared in air atmosphere in capillary tubes. The irradiation (0.7–21 mn), was directly done into the EPR cavity while the spectrum is recording using a Thorlab LED450nm as a light source. EPR assays were all carried out at room temperature using a Bruker E500 spectrometer operating at X-band (9.44 GHz), with 100 KHz modulation frequency. The instrument settings were as follows: microwave power; 2-69 mW; modulation amplitude; 1 G; Hyperfine coupling constants a and g values were obtained with simulation of experimental spectra using easyspin (Matlab toolbox). Gaussian16 code was used to optimize the geometries at the ground and excited states along with the global hybrid functional PBE0. This functional was chosen because of its accuracy to reproduce spectroscopic properties of BTI-based molecules. Structural optimizations and subsequent frequency calculations for both the ground and excited states were performed using an all electron Pople triple zeta basis set with one polarization function on all atoms and one diffuse function of heavier atoms, known as 6-311 + G(d,p), for H, C, N, O and S atoms. Bulk solvent effects were included using the Polarizable Continuum Model (PCM) of Tomasi and co-workers. Default radii (from the UFF, scaled by 1.1) were used. Excited state geometry was obtained by minimizing the forces of the S1 state computed at the TD-DFT level by considering the 3 first excited states. The Orca program was used to compute the SOC between the three first triplet states (namely T1 and T2) and the S1 state at the S1 optimized geometry using the quadric-response TD-DFT at the PBE0/PCM level with the Def2-TZVP basis set adapted for the Douglas-Kroll calculations. The spin-orbit coupling was computed using the Douglas-Kroll Hamiltonian along with the spin-orbit mean field approach. The S1-T1 and S1-T2 energy difference was obtained by CIS(D) calculations with the ORCA software using the Def2-TZVP basis set based on previous benchmark calculations. Crystallographic data were collected on a Rigaku Oxford Diffraction SuperNova diffractometer equipped with an Atlas CCD detector and micro-focus Cu-K_α radiation ($\lambda = 1.54184$ Å). The structure was solved by dual-space algorithm and refined on F^2 by full matrix least-squares techniques using SHELX package (G.M. Sheldrick, ShelXT2018/2, ShelXL2018/3). All non-hydrogen atoms were refined anisotropically and the H atoms were included in the calculation without refinement. Multiscan empirical absorption was corrected by using CrysAlisPro program (CrysAlisPro, Rigaku Oxford Diffraction, V1.171.41.118a, 2021). Deposition Number(s) **2333785** (for **MBTI**) and **2083265** (for **BTI**) contain(s) the supplementary crystallographic data for this paper. These data are provided free of charge by the joint Cambridge Crystallographic Data Centre and Fachinformationszentrum Karlsruhe Access Structures service.

Synthetic procedure: **BTI** was synthetized according to a procedure reported by our group.[23] Synthesis of **1:** 4-methylbenzo[*d*]thiazol-2-amine (5 g, 1 eq) and sodium hydroxide (12.18 g, 10 eq) were charged into a 250 mL round bottom flask equipped with a condenser. A mixture of ethylene glycol and water (100 mL, 9/1 V/V) was added and the flask was heated to 180 °C overnight. After cooling down to r. t., the reaction mixture was quenched with acetic acid until pH ≈ 5. This phase was then extracted with diethyl ether (3×30 mL). The ethereous solution was washed with water (2×50 mL), brine (1×50 mL), dried over $MgSO_4$ and concentrated in vacuo. The crude product was purified on a short plug of silica using dichloromethane as eluent affording a pale-yellow solid (2.71 g, 64 % yield). ^{1}H NMR (300 MHz, $CDCl_3$): δ 7.14–6.91 (m, 2H), 6.52 (t, J = 7.6 Hz, 1H), 4.33 (s, 2H), 2.17 (s, 3H). Synthesis of **MBTI:** 4-bromo-1,8-naphthalic anhydride (200 mg, 1 eq), 2-amino-3-methyl-benzenethiol **1** (110 mg, 1.1 eq) and potassium carbonate (50 mg, 0.5 eq) were placed into a 5 mL pressure vial equipped with a stir bar. 2-ethoxyethanol (4 mL) was added to the powders and the tube was sealed before being inserted into the cavity of a Biotage Initiator + where it was subjected to microwave irradiations for one hour when reaching 150 °C. After cooling down to r. t., isoamyl nitrite (0.338 mL, 3 eq) was added with syringe through the cap's septum. The color of the mixture instantly changed from yellow to orange. The tube was irradiated again to 150 °C for 1.5 hour. After a cooling cycle, 3-aminopentane (0.168 mL, 2 eq) as added to the mixture and the tube irradiated one last time to 150 °C for 3 hours. After cooling down to r. t., the mixture was diluted with dichloromethane (≈ 30 mL) and this organic phase was washed with water (2×) and brine (1×). The organic phase was dried over $MgSO_4$ and concentrated by rotary evaporation. The crude product was then purified on silica gel column chromatography using dichloromethane as eluent affording **MBTI** as an orange powder (84 mg, 30 % yield with regards to the starting naphthalic anhydride). ^{1}H NMR (300 MHz, $CDCl_3$) δ 8.60 (d, *J* = 8.1 Hz, 1H), 8.41 (d, *J* = 7.9 Hz, 1H), 7.97 (d, *J* = 8.1 Hz, 1H), 7.53 (d, *J* = 7.9 Hz, 1H), 7.29 (m, 3H), 5.15–4.98 (m, 1H), 2.74 (s, 3H), 2.37–2.14 (m, 2H), 1.91 (tt, *J* = 13.3, 7.4 Hz, 2H), 0.90 (t, *J* = 7.5 Hz, 6H). ^{13}C NMR (75 MHz, $CDCl_3$) δ 139.48, 138.57, 137.06, 134.28, 132.23, 129.88, 129.24, 128.90, 128.33, 126.59, 124.21, 120.18, 57.46, 25.48, 25.10, 11.46. HRMS (EI) calculated for $C_{24}H_{21}NO_2S$ 387.1293, found 387.1286 (Δ = −1.8 ppm)

Supporting information

The authors have cited the additional reference within the Supporting Information.[29]

Nuclear Magnetic Resonance (NMR), High Resolution Mass Spectrometry (HRMS), absorption and emission, EPR spectra, crystallographic data and electrochemical H2O2 measurements are available in the SI.

Acknowledgements

D. P. S. and C.C. acknowledge the MITI of the CNRS and the ANR (BTXI-Apogee, ANR-20-CE05-0029), respectively. T.L.B. acknowledges the Institut Universitaire de France for funding and the SYSPROD project and AXELERA Pôle de Compétitivité for financial support (PSMN Data Center). This study received the support of the EUR LUMOMAT (*programme Investissements d'Avenir* ANR-18-EURE-0012).

Conflict of Interests

The authors declare no conflict of interest.

Data Availability Statement

The data that support the findings of this study are available in the supplementary material of this article.

Keywords: Dye chemistry · benzothioxanthene imide · structure-property relationships · intersystem crossing · spin-orbit coupling

[1] a) V.-N. Nguyen, S. Qi, S. Kim, N. Kwon, G. Kim, Y. Yim, S. Park, J. Yoon, *J. Am. Chem. Soc.* **2019**, *141*, 16243–16248; b) P. Majumdar, R. Nomula, J. Zhao, *J. Mater. Chem. C* **2014**, *2*, 5982–5997.
[2] a) X. Zhao, Y. Hou, L. Liu, J. Zhao, *Energy Fuels* **2021**, *35*, 18942–18956; b) N. F. Nikitas, P. L. Gkizis, C. G. Kokotos, *Org. Biomol. Chem.* **2021**, *19*, 5237–5253.
[3] a) D. Tzeli, I. D. Petsalakis, *J. Chem.* **2019**, *2019*, 6793490; b) I. S. Turan, G. Gunaydin, S. Ayan, E. U. Akkaya, *Nat. Commun.* **2018**, *9*, 805.
[4] a) D. A. Markelov, V. P. Kozinenko, S. Knecht, A. S. Kiryutin, A. V. Yurkovskaya, K. L. Ivanov, *Phys. Chem. Chem. Phys.* **2021**, *23*, 20936–20944; b) S. Liu, H. Liu, Y. Hu, C. Zhao, H. Huang, G. Yu, Z. Li, Z. Liu, Y. Chen, X. Li, *Chem. Eng. J.* **2023**, *452*, 139203.
[5] a) X. Xiao, W. Tian, M. Imran, H. Cao, J. Zhao, *Chem. Soc. Rev.* **2021**, *50*, 9686–9714; b) T. N. Singh-Rachford, F. N. Castellano, *Coord. Chem. Rev.* **2010**, *254*, 2560–2573.
[6] a) M. Lan, S. Zhao, W. Liu, C.-S. Lee, W. Zhang, P. Wang, *Adv Healthc Mater.* **2019**, *8*, 1900132; b) S. Monro, K. L. Colón, H. Yin, J. Roque, III, P. Konda, S. Gujar, R. P. Thummel, L. Lilge, C. G. Cameron, S. A. McFarland, *Chem. Rev.* **2019**, *119*, 797–828.
[7] V.-N. Nguyen, Y. Yan, J. Zhao, J. Yoon, *Acc. Chem. Res.* **2021**, *54*, 207–220.
[8] a) D. Huang, J. Sun, L. Ma, C. Zhang, J. Zhao, *Photochem. Photobiol. Sci.* **2013**, *12*, 872–882; b) M. Hussain, J. Zhao, W. Yang, F. Zhong, A. Karatay, H. G. Yaglioglu, E. A. Yildiz, M. Hayvali, *J. Lumin.* **2017**, *192*, 211–217.
[9] K. Nobuaki, *BCSJ* **1982**, *55*, 3093–3096.
[10] B. Ventura, G. Marconi, M. Bröring, R. Krüger, L. Flamigni, *New J. Chem.* **2009**, *33*, 428–438.
[11] Y. Hou, X. Zhang, K. Chen, D. Liu, Z. Wang, Q. Liu, J. Zhao, A. Barbon, *J. Mater. Chem. C* **2019**, *7*, 12048–12074.
[12] M. Hussain, A. M. El-Zohry, Y. Hou, A. Toffoletti, J. Zhao, A. Barbon, O. F. Mohammed, *J. Phys. Chem. B* **2021**, *125*, 10813–10831.
[13] a) K. Schmidt, S. Brovelli, V. Coropceanu, D. Beljonne, J. Cornil, C. Bazzini, T. Caronna, R. Tubino, F. Meinardi, Z. Shuai, J.-L. Brédas, *J. Phys. Chem. A* **2007**, *111*, 10490–10499; b) M. Deiana, J. M. Andrés Castán, P. Josse, A. Kahsay, D. P. Sánchez, K. Morice, N. Gillet, R. Ravindranath, A. K. Patel, P. Sengupta, I. Obi, E. Rodriguez-Marquez, L. Khrouz, E. Dumont, L. Abad Galán, M. Allain, B. Walker, H. S. Ahn, O. Maury, P. Blanchard, T. Le Bahers, D. Öhlund, J. von Hofsten, C. Monnereau, C. Cabanetos, N. Sabouri, *Nucleic Acids Res.* **2023**, *51*, 6264–6285.
[14] a) M. Koli, S. Gupta, S. Chakraborty, A. Ghosh, R. Ghosh, A. P. Wadawale, T. K. Ghanty, B. S. Patro, S. Mula, *Chem. Eur. J.* **2023**, *29*, e202301605; b) Y. Yan, A. A. Sukhanov, M. H. E. Bousquet, Q. Guan, J. Zhao, V. K. Voronkova, D. Escudero, A. Barbon, Y. Xing, G. G. Gurzadyan, D. Jacquemin, *J. Phys. Chem. B* **2021**, *125*, 6280–6295.
[15] a) L. A. Ortiz-Rodríguez, C. E. Crespo-Hernández, *Chem. Sci.* **2020**, *11*, 11113–11123; b) M. Deiana, P. Josse, C. Dalinot, A. Osmolovskyi, P. S. Marqués, J. M. A. Castán, L. Abad Galán, M. Allain, L. Khrouz, O. Maury, T. Le Bahers, P. Blanchard, S. Dabos-Seignon, C. Monnereau, N. Sabouri, C. Cabanetos, *Commun. Chem.* **2022**, *5*, 142.
[16] a) P. Josse, S. Li, S. Dayneko, D. Joly, A. Labrunie, S. Dabos-Seignon, M. Allain, B. Siegler, R. Demadrille, G. C. Welch, C. Risko, P. Blanchard, C. Cabanetos, *J. Mater. Chem. C* **2018**, *6*, 761–766; b) J. M. Andrés Castán, L. Abad Galán, S. Li, C. Dalinot, P. Simón Marqués, M. Allain, C. Risko, C. Monnereau, O. Maury, P. Blanchard, C. Cabanetos, *New J. Chem.* **2020**, *44*, 900–905; c) C. Dalinot, P. Simón Marqués, J. M. Andrés Castán, P. Josse, M. Allain, L. Abad Galán, C. Monnereau, O. Maury, P. Blanchard, C. Cabanetos, *Eur. J. Org. Chem.* **2020**, *2020*, 2140–2145; d) P. Simón Marqués, J. M. Andrés Castán, L. A. Galan, M. Allain, O. Maury, T. Le Bahers, P. Blanchard, C. Cabanetos, *J. Org. Chem.* **2021**, *86*, 5901–5907.
[17] a) J. M. Andrés Castán, C. Dalinot, S. Dayneko, L. Abad Galan, P. Simón Marqués, O. Alévêque, M. Allain, O. Maury, L. Favereau, P. Blanchard, G. C. Welch, C. Cabanetos, *Chem. Commun.* **2020**, *56*, 10131–10134; b) A.-J. Payne, N. A. Rice, S. M. McAfee, S. Li, P. Josse, C. Cabanetos, C. Risko, B. H. Lessard, G. C. Welch, *ACS Appl. Energ. Mater.* **2018**.
[18] a) J. M. A. Castán, C. Amruth, P. Josse, L. A. Galan, P. S. Marqués, M. Allain, O. Maury, T. Le Bahers, P. Blanchard, C. Monnereau, G. C. Welch, C. Cabanetos, *Mater. Chem. Front.* **2022**; b) A. L. Dauphin, J. M. Andrés Castán, J. Yu, P. Blanchard, N. Sojic, H. S. Ahn, B. Walker, C. Cabanetos, L. Bouffier, *ChemElectroChem* **2022**, *9*, e202200967.
[19] a) L. A. Galán, J. M. Andrés Castán, C. Dalinot, P. S. Marqués, P. Blanchard, O. Maury, C. Cabanetos, T. Le Bahers, C. Monnereau, *Phys. Chem. Chem. Phys.* **2020**, *22*, 12373–12381; b) D. P. Sánchez, P. Josse, M. G. Mutovska, B. Siegler, M. Allain, K. Morice, P. Blanchard, F. Gohier, T. Le Bahers, C. Monnereau, Y. Zagranyarski, D. Lungerich, C. Cabanetos, *ChemistryEurope* **2024**, *2*, e202300071.
[20] M. Deiana, J. M. Andrés Castán, P. Josse, A. Kahsay, D. P. Sánchez, K. Morice, N. Gillet, R. Ravindranath, A. K. Patel, P. Sengupta, I. Obi, E. Rodriguez-Marquez, L. Khrouz, E. Dumont, L. Abad Galán, M. Allain, B. Walker, H. S. Ahn, O. Maury, P. Blanchard, T. Le Bahers, D. Öhlund, J. von Hofsten, C. Monnereau, C. Cabanetos, N. Sabouri, *Nucleic Acids Res.* **2023**.
[21] D. Sasikumar, A. T. John, J. Sunny, M. Hariharan, *Chem. Soc. Rev.* **2020**, *49*, 6122–6140.
[22] M. Imran, H. Cao, J. Zhao, G. Mazzone, *J. Phys. Chem. A* **2023**, *127*, 4856–4866.
[23] P. Josse, K. Morice, D. Puchán Sánchez, T. Ghanem, J. Boixel, P. Blanchard, C. Cabanetos, *New J. Chem.* **2022**, *46*, 8393–8397.
[24] T. Le Bahers, C. Adamo, I. Ciofini, *J. Chem. Theory Comput.* **2011**, *7*, 2498–2506.
[25] a) C. Mendoza, A. Désert, L. Khrouz, C. A. Páez, S. Parola, B. Heinrichs, *Environ. Sci. Pollut. Res. Int.* **2021**, *28*, 25124–25129; b) G. Nardi, I. Manet, S. Monti, M. A. Miranda, V. Lhiaubet-Vallet, *Free Radical Biol. Med.* **2014**, *77*, 64–70.
[26] a) G. R. Buettner, *Free Radical Res. Commun.* **1993**, *19*, s79-s87; b) P. Bilski, K. Reszka, M. Bilska, C. F. Chignell, *J. Am. Chem. Soc.* **1996**, *118*, 1330–1338.
[27] G. R. Buettner, *Free Radical Biol. Med.* **1987**, *3*, 259–303.
[28] a) P. Gostinis, K. Berg, Cengel, K. A. T. H. Foster, A. W. Girotti, S. O. Gollnick, S. M. Hahn, M. R. Hamblin, A. Juzeniene, D. Kessel, M. Korbelik, J. Moan, P. Mroz, D. Nowis, J. Piette, B. C. Wilson, J. Golab, *CA Cancer J Clin* **2011**, *61*, 250–281; b) T. C. Pham, V. N. Nguyen, Y. Choi, S. Lee, J. Yoon, *Chem. Rev.* **2021**, *121*, 13454–13619.
[29] P. Pieta, A. Petr, W. Kutner, L. Dunsch, *Electrochim. Acta* **2008**, *53*, 3412–3415.

Manuscript received: January 16, 2024
Accepted manuscript online: March 18, 2024
Version of record online: April 11, 2024